

Article

Study on Properties of High-Vanadium Full-Locked Cable with Alloy Coating with Defects

Zhou Fang ^{1,*} , Junjie Fu ¹, Zhe Wang ², Binlei Chen ², Puan Shi ¹ and Jiahao Ma ¹

¹ College of Mechanical and Electrical Engineering, Beijing University of Chemical Technology, Beijing 100029, China; jifu@buct.edu.cn (J.F.); 2020200637@buct.edu.cn (P.S.); refinedma@163.com (J.M.)

² Beijing Institute of Architectural Design, Beijing 100045, China; wangzhe3@biad.com.cn (Z.W.); binleic@126.com (B.C.)

* Correspondence: zhoufang@buct.edu.cn

Abstract: The Zn-5%Al-rare earth alloy coating has been used in High-Vanadium Full-Locked Cable (HVFLC) that is made in China. This application has shown excellent protective performance. However, during practical use, the coating may appear to be deteriorated in various degrees, which may further worsen the corrosion resistance and mechanical properties of the cable. This paper focuses on High-Vanadium Full-Locked Cable (HVFLC). Firstly, different types of prefabricated defect treatments have been applied into the wires of the cable, followed by corrosion paste accelerated corrosion test and mechanical tensile properties test. The aim of this act is to figure out the effects on the corrosion resistance and mechanical properties of the wire due to different types of defects in alloy plating. The results show that the corrosion resistance of the wires has been greatly affected because of the solder joint defects. Furthermore, the tensile strength of the wire indicates a drop of about 40%. This research makes up the gap in the related fields in China. In addition, basic data has been provided for the development of the HVFLC in China.

Keywords: defects; Zn-5%Al-rare earth alloy coating; high-vanadium full-locked cable (HVFLC) made in China; performance



Citation: Fang, Z.; Fu, J.; Wang, Z.; Chen, B.; Shi, P.; Ma, J. Study on Properties of High-Vanadium Full-Locked Cable with Alloy Coating with Defects. *Processes* **2022**, *10*, 513. <https://doi.org/10.3390/pr10030513>

Academic Editor: Prashant K Sarswat

Received: 10 February 2022

Accepted: 1 March 2022

Published: 4 March 2022

Publisher's Note: MDPI stays neutral with regard to jurisdictional claims in published maps and institutional affiliations.



Copyright: © 2022 by the authors. Licensee MDPI, Basel, Switzerland. This article is an open access article distributed under the terms and conditions of the Creative Commons Attribution (CC BY) license (<https://creativecommons.org/licenses/by/4.0/>).

1. Introduction

The 24th Winter Olympic Games, a grand event attracting worldwide attention, will be held in Beijing, China in 2022. The National Speed Skating Oval (NSSO) was established in Beijing to meet the requirements of a competition venue for the Winter Olympics. The NSSO became a new landmark building after Bird's Nest and Water Cube in Beijing. The NSSO is also known as "the ice ribbon" due to its appearance as a ribbon (Figure 1). The NSSO is the highest level of architectural design for large venues in China. It has shown the strength of China's construction industry to the world and made major breakthroughs in some fields. The most remarkable achievement is the application of the HVFLC, which forms the cable network structure of the roof of the stadium. The NSSO adopts the roof design of hyperboloid saddle-shaped single-layer cable net structure (Figure 2), which is the largest single-layer bidirectional orthogonal saddle shape cable net roof stadium in the world [1–3]. It is also the first application of HVFLC in the construction of a large venue in China.

Due to the high manufacturing difficulties of the HVFLC, the market in China has been occupied by Europe, the United States, Japan and other developed countries for a long time. The HVFLC is very expensive in China. In recent years, technological breakthroughs have been made in the research and development of the HVFLC in China. The HVFLC with excellent performance has been produced by domestic manufacturers in China. Additionally, it can be used in the construction of the NSSO [4]. However, the HVFLC has never been used in the practical engineering of large-scale architecture field before. There is no

systematic research on durability and long-term performance of the HVFLC during service. There are gaps in the basic data.



Figure 1. The National Speed Skating Oval (NSSO).



Figure 2. The roof of the cable mesh structure.

The HVFLC has obvious differences from the ordinary cable in the structure. The structure is shown in Figure 3. The HVFLC adopts a double-layer structure. The inner layer is twisted around wire, and the outer layer is multi-strand Z-type wire to form a fully closed structure. The HVFLC has excellent properties such as high axial stiffness, low elongation, and not easy to jump [5]. It is very suitable for building structures as the main force-bearing material. The surface of each wire of the HVFLC is coated with Zn-5%Al-rare earth alloy. The alloy coating has excellent corrosion resistance, which is about 2–3 times higher than that of ordinary galvanized coatings. In harsh environments such as outdoor, humid environments and marine climates, the alloy coating has better corrosion resistance than ordinary hot-dip galvanizing and electro-galvanizing. The presence of alloy plating plays an important role in the corrosion resistance of steel wires. The effectiveness of the alloy coating is a key factor affecting the serviceability and longevity of the steel cable. However, the alloy coating may be damaged during the construction process, such as scratches, abrasion, and welding spots (Figure 4).

Alloy plating, as a protective measure, is essential to ensure the long-term performance of the cable. As can be expected, defects and damage caused during processing and installation can affect the performance of the cable. The specific effects need to be further studied. However, the HVFLC is not yet industrialized, and there are few related studies.

In this paper, the performance of HVFLC wires in the presence of damage is investigated. The damage behavior of the Zn-5%Al-rare earth alloy coating during processing and installation was considered. The corrosion behavior of the damaged alloy coating in a corrosive environment and the specific effects of the damage on the corrosion resistance and mechanical properties of the cable were studied. Accelerated laboratory corrosion tests were performed. The coupling effects of temperature, humidity and initial damage were considered. The effect of the Zn-5% Al-rare earth alloy coating on the cable serviceabil-

ity under different damage conditions was investigated. In addition, a corrosion safety assessment method for HVFLC was explored.

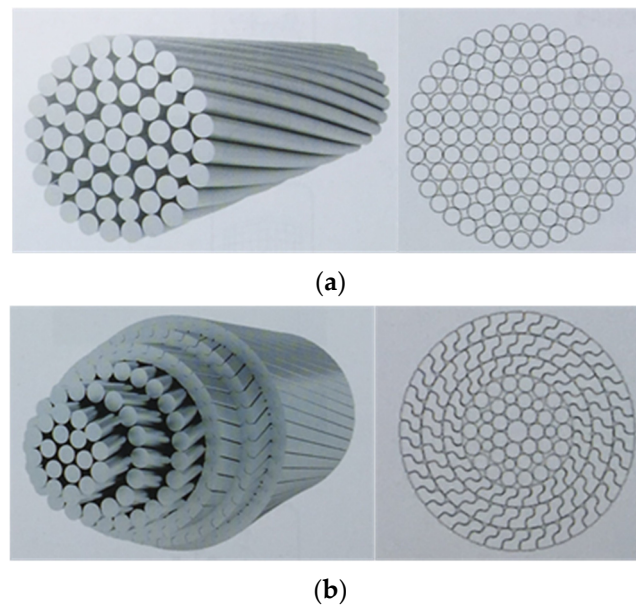


Figure 3. The schematic diagrams of ordinary cable structure and high vanadium closed cable structure. (a) The structure of an ordinary cable, and (b) the structure of the HVFLC.

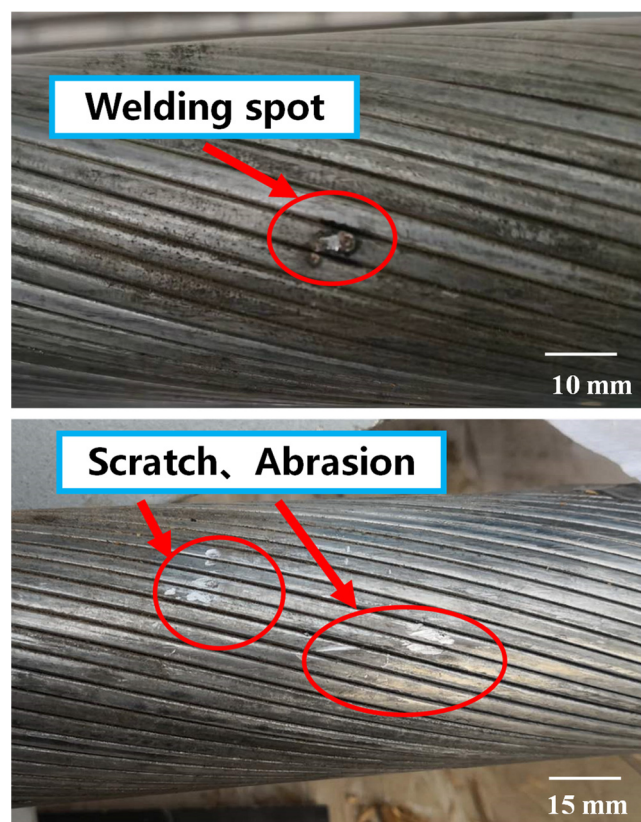


Figure 4. Damage mode of alloy coating.

2. Experimental

2.1. Design and Manufacture of Specimen

The HVFLC is made of different types of steel wires twisted by applying pre-stress. Each wire is an important component of the cable. In this study, the HVFLC wires with Zn-5%Al-rare earth alloy coating were used as test specimens. A total of 216 specimens were used in the test, including 54 wires with Z-sections of 2.6 mm, 4.0 mm and 5.0 mm round section diameters. The length of all specimens is 260 ± 5 mm. The weight of Z-section specimen is 45 ± 1 g. The weight of $\phi 2.6$ mm specimen is 11 ± 1 g. The weight of $\phi 4.0$ mm specimen is 28 ± 1 g. The weight of $\phi 2.6$ mm specimen is 41 ± 1 g. The average thickness of the coating on the surface of the specimen is 80–170 μm .

The specimens include two types of steel wires with Z-section and round section. The round section wire specimens are available in three different sizes $\phi 2.6$ mm, $\phi 4.0$ mm and $\phi 5.0$ mm. Three types of defective specimens, namely scratches, abrasions and welding spots, were produced to take into account the damage that may occur in the actual use of the HVFLC. According to the diversity of scratch defects, three types of axial scratches, radial scratches and spiral scratches were produced. All types of specimens are shown in Figure 5. The specimens can be divided into normal specimen group, scratch defect group, abrasion defect group and welding spot defect group. Each group has three specimens, and the test data are averaged.

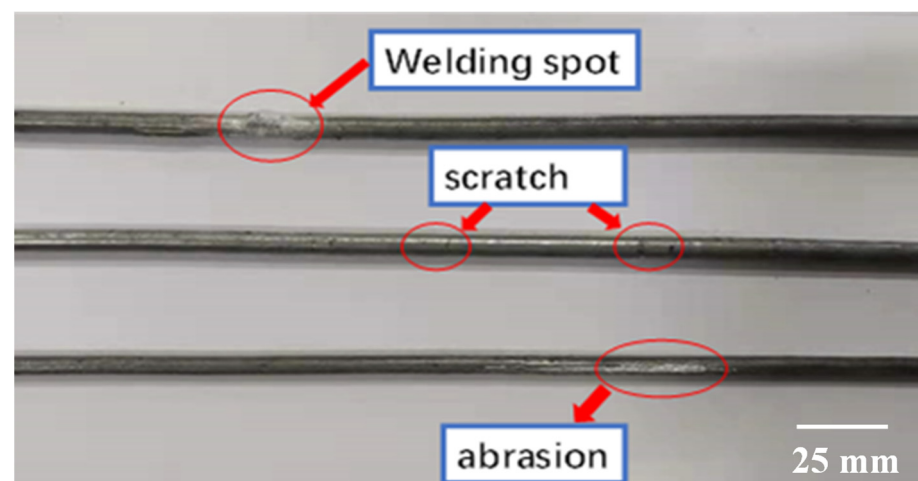


Figure 5. Schematic of defective specimen.

In order to compare and analyze the data of each group of specimens, the specimens were named according to their differences. The naming method of each group of specimens is section type-diameter-defect type-number. The specific naming is shown in Table 1. In addition, “00, 45, and 90” in $\phi 50\text{-S-00/45/90-1/2/3}$ represent three different angles of axial, spiral and radial scratch defects. Each set of specimens was washed several times with anhydrous ethanol before testing to remove the organic matter adhering to the surface.

Table 1. List of specimen names.

Section	Diameter	Defects	Serial Number
Z	5H	N/A/S00/S45/S90/W	1/2/3/4/5/6
O	26	N/A/S00/S45/S90/W	1/2/3/4/5/6
O	40	N/A/S00/S45/S90/W	1/2/3/4/5/6
O	50	N/A/S00/S45/S90/W	1/2/3/4/5/6

2.2. Experimental Materials and Instruments

The drugs used in the corrosion paste test are shown in Table 2. The equipment used in the test included damp chamber, small air compressor, etc.

Table 2. Chemical composition of corrosive paste.

Name	Specification	Manufacturer
Cu(NO ₃) ₂ ·3H ₂ O	AR 99.9%	Macklin
FeCl ₃ ·6H ₂ O	AR 99%	Macklin
NH ₄ Cl	AR 99.9%	Macklin
Kaolin	CP	Macklin
Ethanol absolute	AR 99.7%	Macklin
Deionized water	/	/

2.3. Experiment for Accelerated Corrosion

- (1) The HVFLC is subject to corrosion from atmospheric conditions during application. Accelerated corrosion test can simulate the effect of long-period atmospheric corrosion in the laboratory. According to GBT 6455-2008 [6], the corrosion paste experiment is used to simulate the accelerated corrosion test.
- (2) Preparation of corrosion paste. 0.035 g of Cu (NO₃)₂·3H₂O (AR), 0.165 g of FeCl₃·6H₂O (AR) and 1.0 g of NH₄Cl (AR) were dissolved in 50.0 mL of distilled water. Then, 30.0 g of kaolinite was added. In order to fully soak the kaolin, the slurry was mixed thoroughly by rapid stirring with a glass rod and allowed to stand for 2 min. Stir well with a glass rod before using.
- (3) Brushing of corrosion paste. Apply the corrosion paste evenly on the specimen. The thickness of the corrosion paste should be between 0.08 mm and 0.20 mm. The specimen is dried at room temperature with relative humidity less than 50% for 1 h, and then placed in a humid room.
- (4) Setting the corrosive environment. The treated specimens are reasonably placed in a damp box. There is no contact between the specimen and the specimen or between the specimen and the wall of the box. The temperature in the test chamber is maintained at 35 ± 1 °C, and the relative humidity is maintained between 80~90%.
- (5) Test period and specimen treatment after testing. Every 24 h is an experimental period. After the test, the specimen is cleaned to remove the corrosion paste from the surface.

2.4. Characterization and Performance Testing

The corrosion pattern of the specimens was analyzed by the loss of weight method. The weight of each specimen after the test was weighed using an electronic balance and compared with the weight of the specimen before the test.

The mechanical tensile properties of the specimens were tested using the Instron 8801 hydraulic servo fatigue testing machine. The differences in mechanical properties before and after the corrosion test were compared and analyzed.

The surface morphology of the corroded specimen and the fracture section of the tensile specimen were observed by a metallographic microscope (RX50M research microscope) and SEM (cold field scanning electron microscope S-4700). The metallographic structure of the specimen was observed with a metallographic microscope. The composition of the corrosion products was analyzed by EDS (cold field scanning electron microscope S-4700).

3. Results and Discussions

3.1. Research on Corrosion Regularity

In order to investigate the regularity of the corrosion effect with time, a group of specimens was taken out every 3 h during the 24 h of the corrosion paste test. The weight of the specimens after the test was measured after treatment. The weight loss method is used to analyze the weight variation of samples with time before and after corrosion during the test. The corrosion weight loss of standard specimens of type Z varies with time within 24 h as shown in Figure 6. It can be seen that the weight loss of the specimen is large in a short time after the test starts. As the test proceeds, the weight loss of the specimen tends to stabilize. It may be due to the fact that after a period of corrosion, the Zn and Al in the coating were oxidized to form a dense oxide film, which hindered the development of

corrosion. In addition, after removing the corrosion paste from the surface of the specimen at different times, it can be observed that the surface of the specimen gradually loses its metallic luster. The surface of the specimen eventually becomes dark black. The gradual loss of metallic color of the specimen surface can also prove the formation of oxide film.

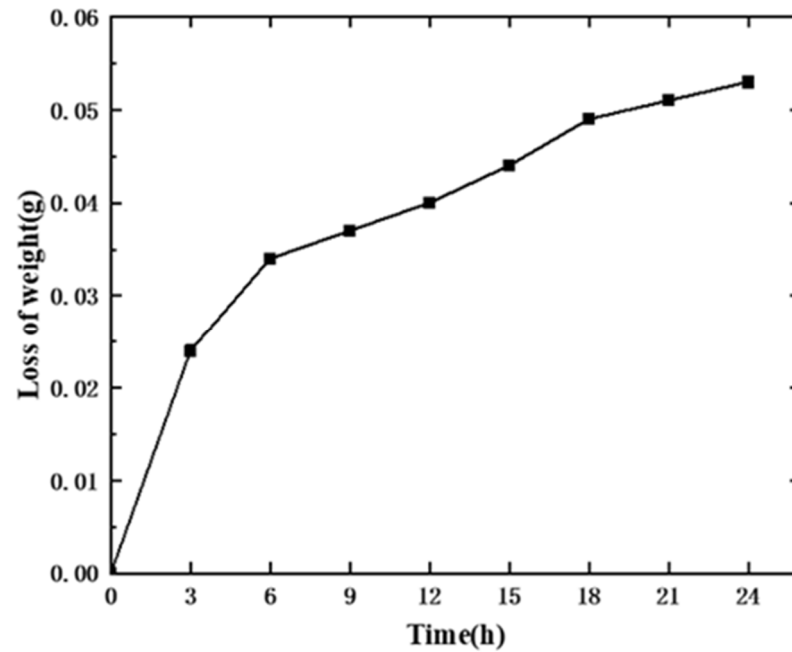


Figure 6. Variation in weight loss of specimens at different times.

The weight variation of the specimen groups with different defects during one test cycle (16 h) is shown in Figure 7.

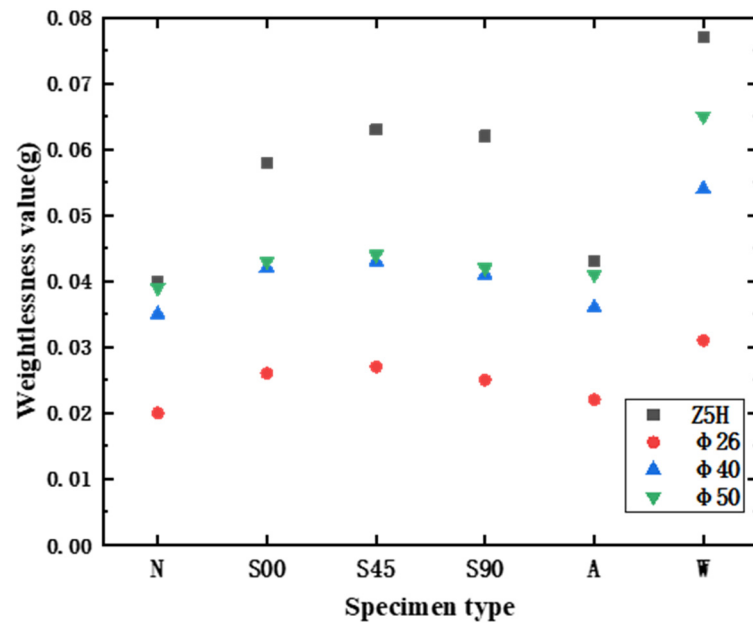


Figure 7. Mass change value of each specimen before and after corrosion.

Some trends can be found in the data. For specimens with circular cross-section, the weight loss of the specimen before and after the corrosion test increases with the diameter. As the diameter of the specimen increases, the contact area between the specimen and the corrosion paste becomes larger, and the corrosion effect is more serious. In addition,

the weight loss of normal specimens was the smallest for both Z-section specimens and circular-section specimens. This indicates that the presence of an intact alloy coating has a good corrosion protection effect. Other defective specimens have different degrees of weight loss increase. Among them, the largest weight loss is the group of welding spot. It can be initially judged that the corrosion effect of the group of welding spot is more serious. Welding spots are formed at high temperatures. The coating in the weld area will be oxidized at high temperature. Additionally, the surface will be rough, white in color and decarburized at high temperature compared with the normal structure (Figure 8). In addition, the high temperature affects the area near the weld, making the actual affected area larger than the surface weld of the specimen [7,8].

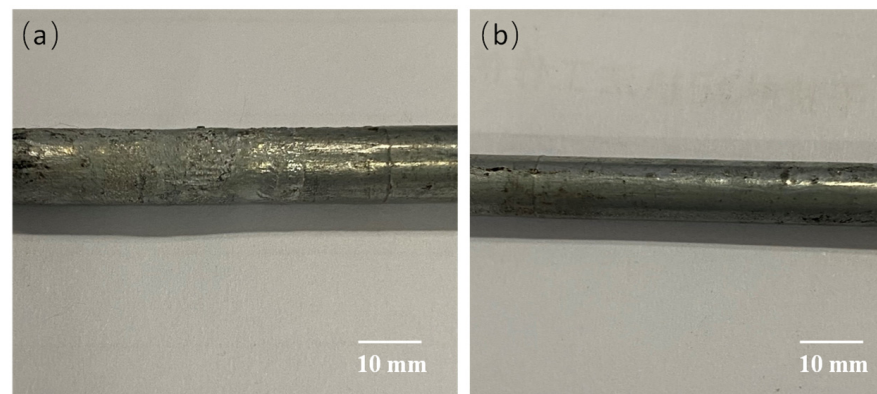


Figure 8. (a) Morphology of weld area of specimen. (b) Morphology of normal area of specimen.

The corrosion products of each group of specimens were scanned and analyzed by EDS. The results are shown in Figure 9. The corrosion products consisted mainly of the elements O, Al, Si, Fe, and Zn. The characteristic peak of Zn was the highest, followed by O. The presence of Si probably due to the fact that the main component of kaolinite is SiO_2 . The mixture of SiO_2 and corrosion products resided on the surface of the specimens [9]. Furthermore, it can be clearly observed that the characteristic peaks of Fe in the normal specimens are not very pronounced in the EDS pattern compared to the other specimens. Fe is probably originated from $\text{FeCl}_3 \cdot 6\text{H}_2\text{O}$ in the corrosion paste. The characteristic peak of Fe is higher in the other specimen groups, which may be due to the damage of the alloy coating causing the corrosion of the corrosion paste on the carbon steel substrate, increasing the Fe content. It could also be due to the damage of the coating that exposed the internal carbon steel substrate. In the group of welding spot, the characteristic peak of Fe is most obvious, indicating a more severe corrosive effect on the carbon steel matrix. In addition, the normal specimen surface intact alloy coating effectively protects the internal carbon steel substrate, so that the corrosive medium does not contact the substrate. Corrosion occurs mainly on the surface of the alloy coating.

The microscopic morphology of each group of specimens after the removal of corrosion products was observed by SEM. The results are shown in Figure 10. The normal specimens had a flat surface with a small number of corrosion pits. Scratch specimens were more severely corroded near the scratch, with more corrosion pits. Abrasion specimens show obvious, but weaker corrosion marks in the abrasion damage area. This may be due to minor abrasion, which does not completely fail the alloy coating. The welding spot specimens had very rough surfaces in the welding spots and adjacent areas. There are many corrosion pits and the corrosion effect is severe. The welding spot defect is very damaging to the alloy coating, making the surface of the alloy coating very rough. In the test, the contact area between the rough surface and the corrosion paste is large. Local corrosion may also occur in the area of the crater, which will worsen the corrosion effect.

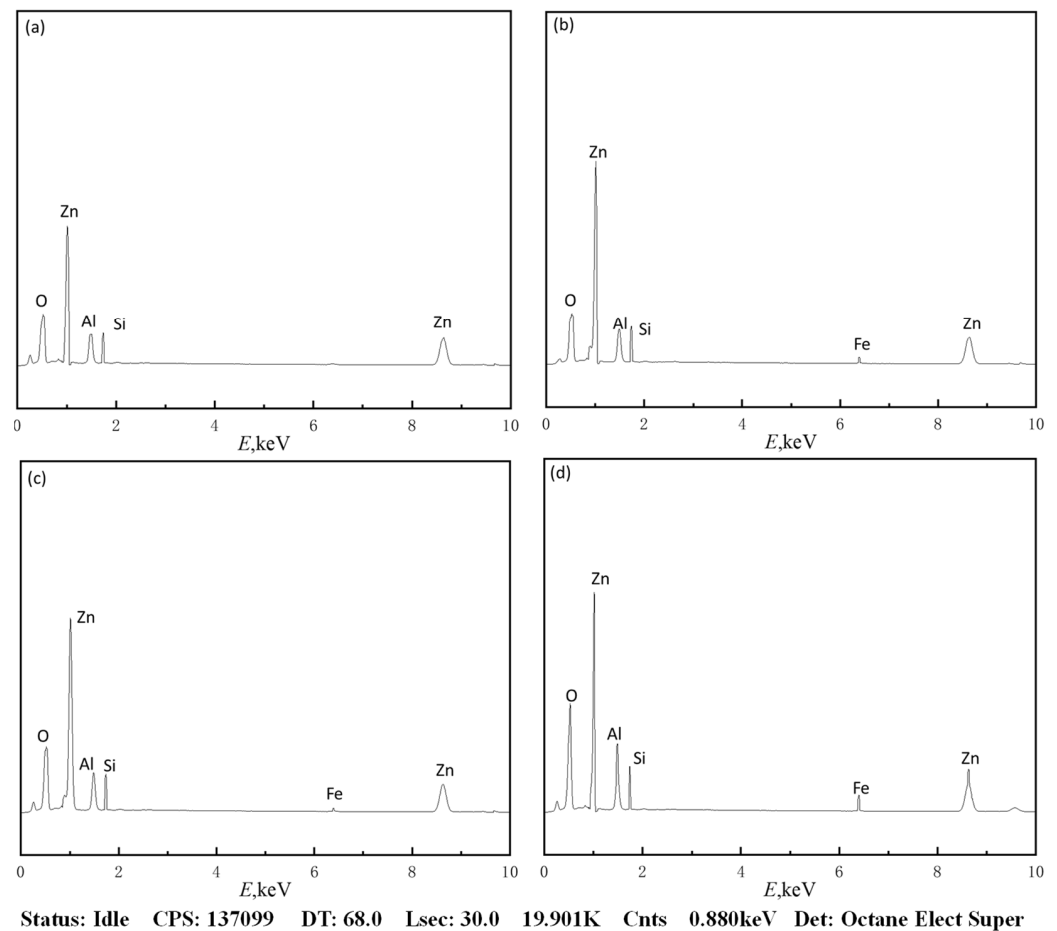


Figure 9. EDS of corrosion products. (a) Normal specimens. (b) Scratched specimens. (c) Abrasion specimens. (d) Welding spot specimens.

In the accelerated corrosion test with corrosive paste, it can be found that the damage of the Zn-5%Al-rare earth alloy coating on the surface of the specimen of the HVFLC has a negative effect on the corrosion protection performance. It can be judged that the defects of welding spots have the most serious impact on the corrosion resistance of the specimens by weight loss analysis, EDS analysis and SEM micro-morphology. In order to ensure the long-term service performance of the HVFLC, It is necessary to avoid the occurrence of welding spots in the actual service environment as far as possible.

3.2. Characterization of Mechanical Properties

Mechanical tensile tests were carried out on the normal specimens group, scratch specimens group, abrasion specimens group and welding spot specimens group with hydraulic servo fatigue tester Instron 8801. Tensile curves of each group were obtained. The tension curve of the Z-section specimen is shown in Figure 11. Tensile curves of $\phi 50$ specimens are shown in Figure 12. Tensile curves of $\phi 40$ specimens are shown in Figure 13. The tensile curves of $\phi 26$ specimen groups are shown in Figure 14.

The tensile curves of the specimens show that the defects of the specimens of the HVFLC have different effects on the mechanical tensile properties of each group of specimens. Scratch defects and abrasion defects had little effect. The tensile curves of welding spot specimens were significantly different from the other specimens. The welding spot specimens fractured at low tensile stresses and short tensile displacements. This indicates that the presence of weld joint defects resulted in a significant change in the specimen properties. The presence of welding spots significantly reduced the mechanical tensile properties of the specimens compared to the other specimens.

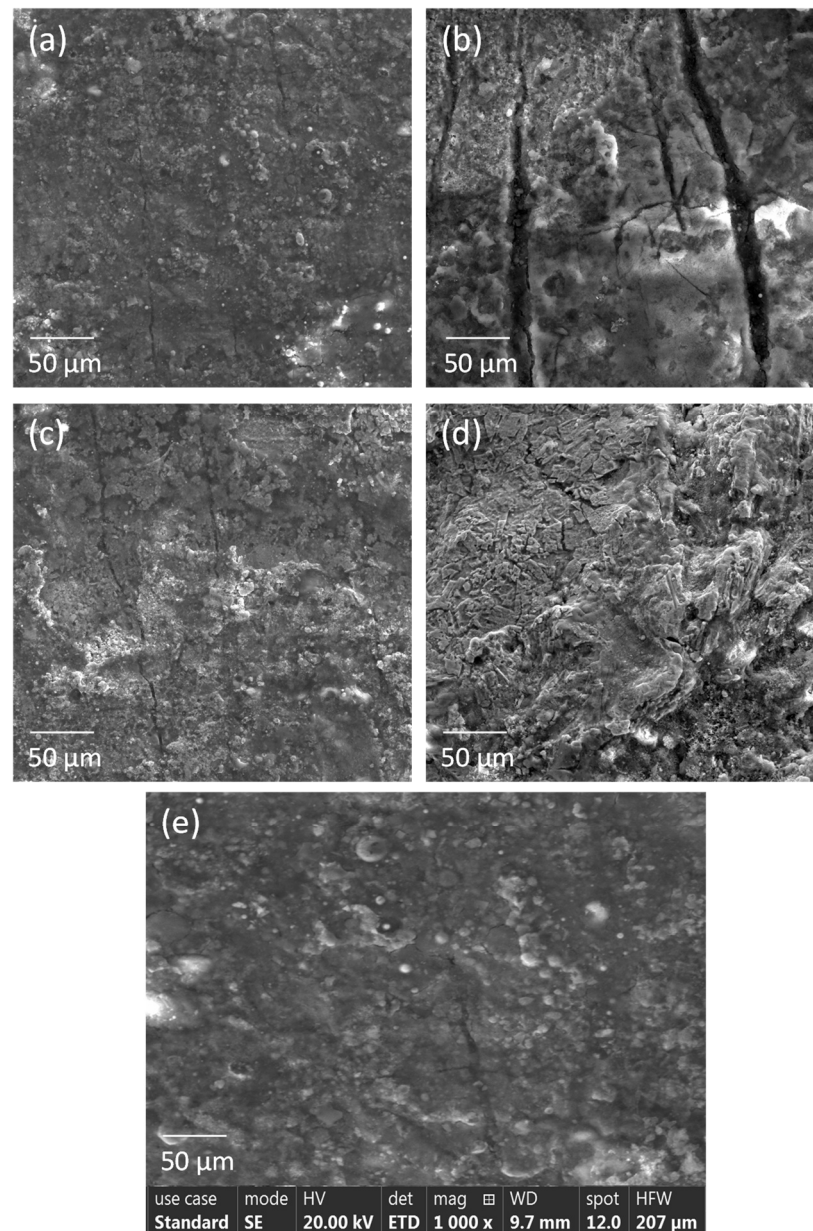


Figure 10. Microscopic morphology of SEM. (a) Normal specimens. (b) Scratched specimens. (c) Abrasion specimens. (d) Welding spot specimens. (e) Microstructure of the specimen before corrosion test.

Tensile strength is an important index for evaluating the mechanical properties of materials. In order to accurately analyze the mechanical properties of the specimens, the tensile strength data of each group of specimens were obtained from the tensile curves of each group (as shown in Figure 15).

From the tensile strength data of each group of specimens, it can be found that the presence of various defects and the effect of corrosion caused the tensile strength of the specimens to weaken to different degrees. The presence of scratch, abrasion, and welding spot reduced the tensile strength of the material compared to the normal specimens with a complete alloy coating. Welding spot defects had the greatest effect, with the tensile strength of the welding spot group of specimens decreasing by about 40% compared to the normal specimens. The intact alloy coating of the standard specimens prevented the material from corroding to a great extent. The presence of various defects makes the wire specimen surface alloy coating damage, so that the corrosive medium can be in direct contact with the metal matrix, corrosion occurs. In addition, the presence of defects in

the welded joints seriously damaged the flatness of the alloy coating. The area where the welding spots exist in the tensile test produces a stress concentration phenomenon, making the specimen very susceptible to fracture in this area (as shown in Figure 16).

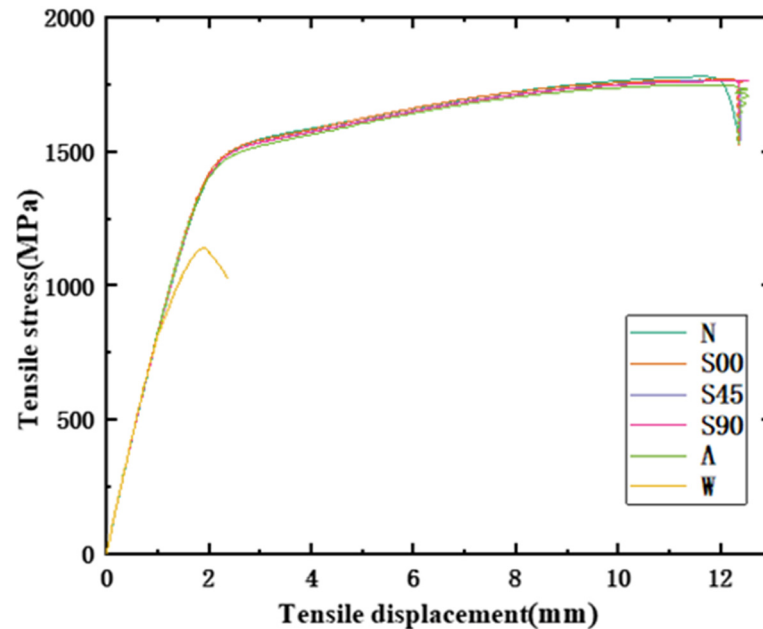


Figure 11. Tensile curve of Z-section specimen.

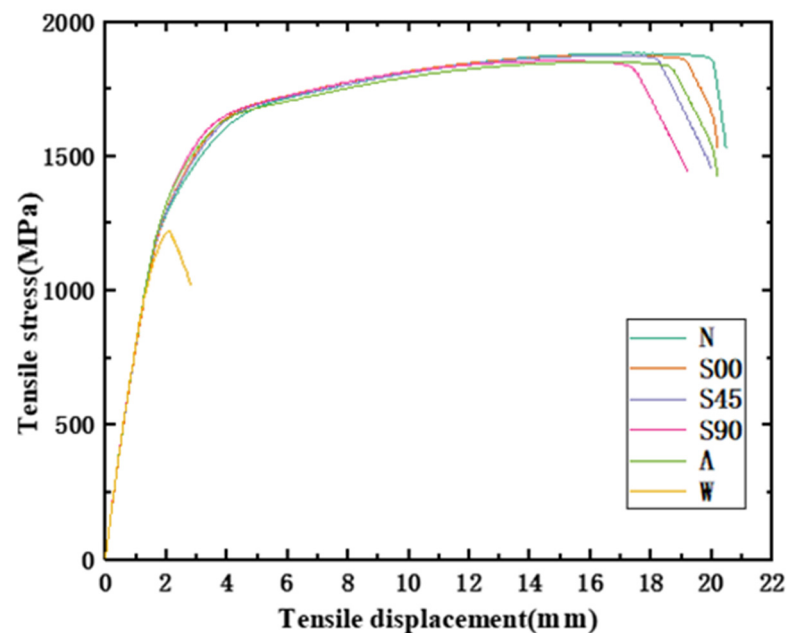


Figure 12. Tensile curve of $\phi 50$ specimen.

The microscopic morphology of the tensile fracture of each group of specimens was observed by SEM. The microscopic morphology of the tensile sections of each group of specimens is shown in Figure 17. It can be seen from Figure 17a–c that the tensile fractures of the normal, scratch and abrasion specimens have obvious ductile fracture characteristics. A necking zone was formed on the fracture surface of the specimens. The tensile fracture region can be observed in the low magnification morphology consisting of the fiber zone, radiation zone and shear lip zone. The fiber zone is rough and fibrous in the center of the fracture. Fracture usually occurs first in the fiber zone and then spreads rapidly to form

the radiation zone. Radial lines are formed during the rapid propagation of the fracture. The junction of the fibrous and radial zones can be seen where the crack transitions from formation to unstable propagation and finally fractures to form a shear lip. The smooth surface of the shear lip indicates the rapid, unstable propagation of the crack. In addition, tough fossa features can be observed under high magnification. Many elongated tough fossae were observed in the microscopic morphology. The size, depth and number of tough nests are closely related to the toughness of the material. The greater the plastic deformability of the material, the greater the depth of the tough fossa.

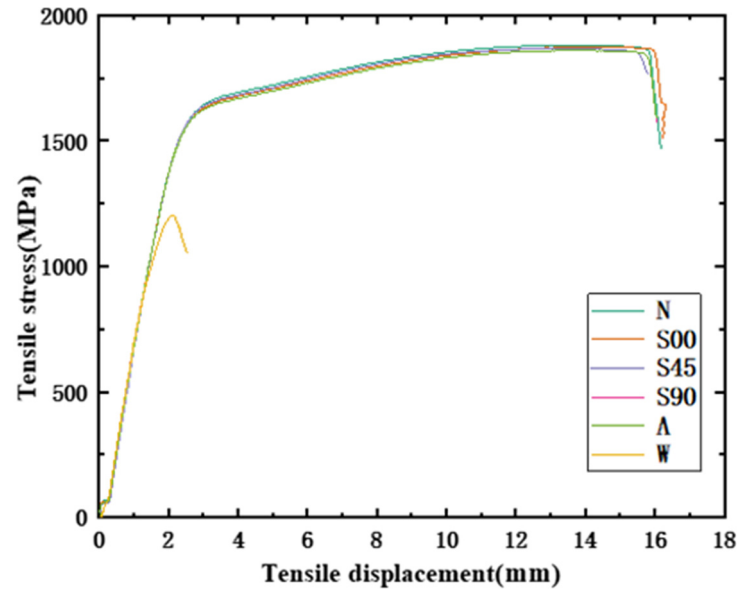


Figure 13. Tensile curve of $\phi 40$ specimen.

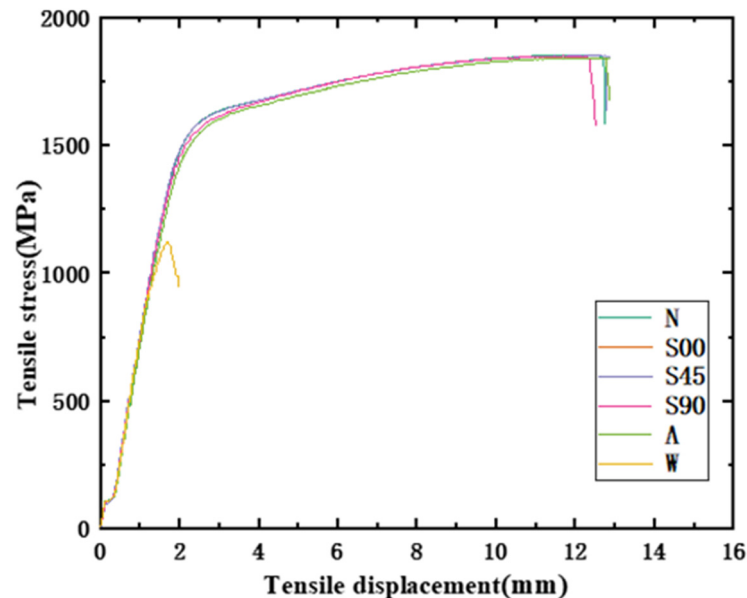


Figure 14. Tensile curve of $\phi 26$ specimen.

The microscopic morphology of the fracture of the welding spot specimen is shown in Figure 17d. It is obvious to observe that the fracture of the welding spot specimen has obvious differences from the fracture of other specimens. There is a necking area at the fracture of the specimen, but there is no obvious ductile fracture feature under the low magnification. The fracture surface is flat and the shear lip is not obvious. The fracture

originates from the lower left edge, corresponding to the weld area on the specimen. In addition, the fracture showing partial toughness fracture characteristics can be observed under high magnification. It can be tentatively concluded that a mixed fracture of ductile fracture and brittle fracture coexisted during the tensile fracture of the group of welding spot specimen.

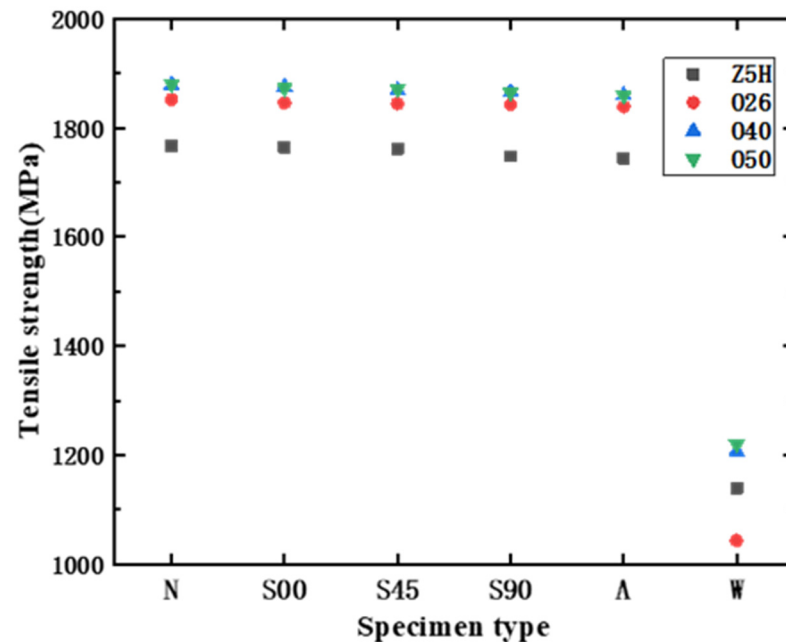


Figure 15. Tensile strength of each specimen group after test.



Figure 16. Fracture location of specimen.

In order to determine the reason for the significant decrease in tensile strength of welding spot specimens, metallographic specimens were taken near the fracture of welding spot break specimens. The metallographic structure is shown in Figure 18. It can be seen that the structure consists of three parts, similar to welding, with welding spots (bumps), heat affected zone, and matrix [10,11]. The structural characteristics of the welding spots (bumps) are shown in Figure 19. It can be seen that the structure has an individual martensite and bainite, while the normal organization of the site is soxhlet (Figure 20). Needle martensite is hard and brittle, has no plastic deformation ability and poor toughness [12]. Additionally, in the process of martensite transformation will make the internal volume expansion, forming a large internal stress. The formation of martensite in the area near the weld joint is the root cause of the brittle fracture of the specimen in the mechanical tensile test. It is also the key factor that causes the decrease in tensile strength of welding spot specimens by about 40%.

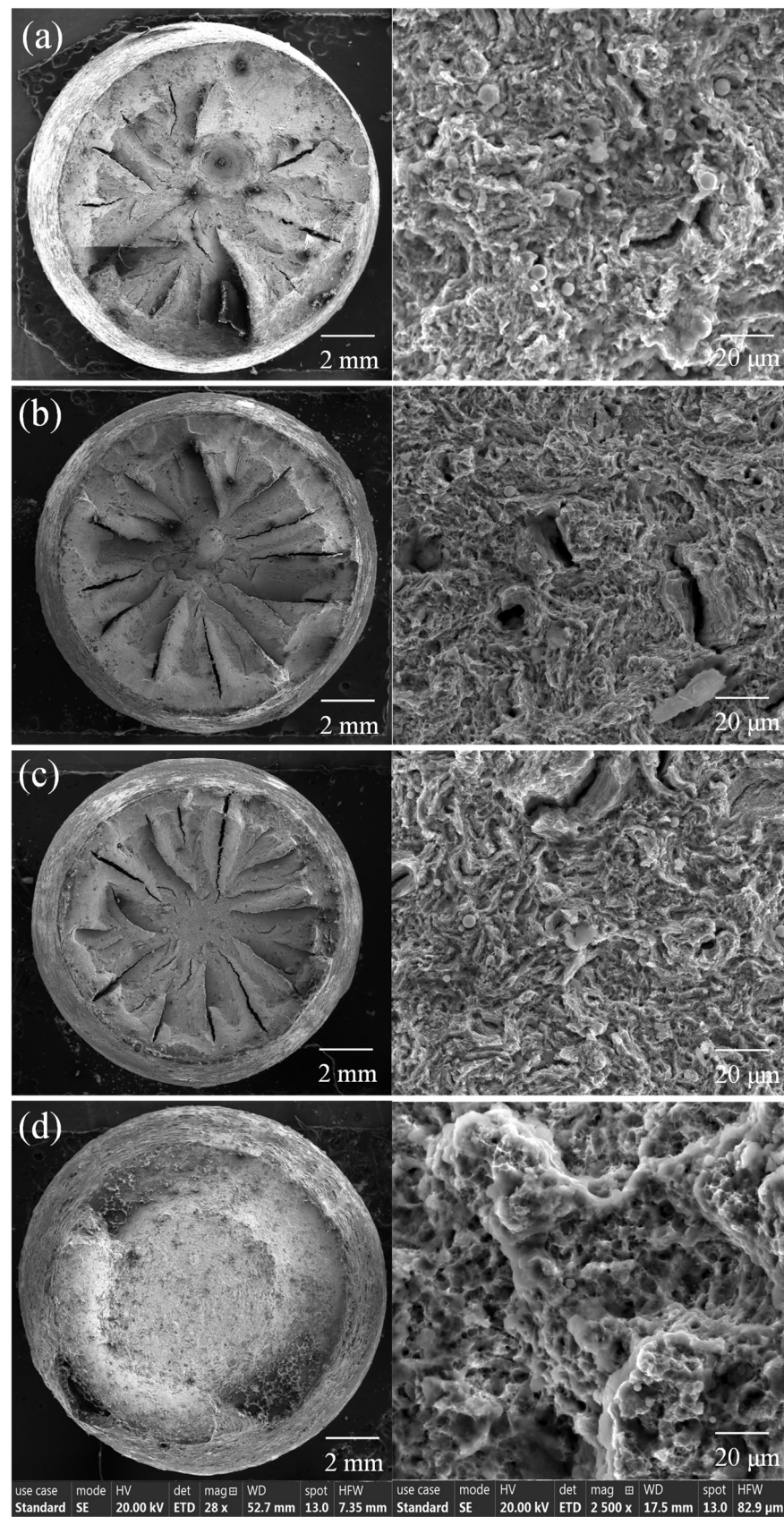


Figure 17. Tensile fracture morphology by SEM. (a) Normal specimens. (b) Scratched specimens. (c) Abrasion specimens. (d) Welding spot specimens.

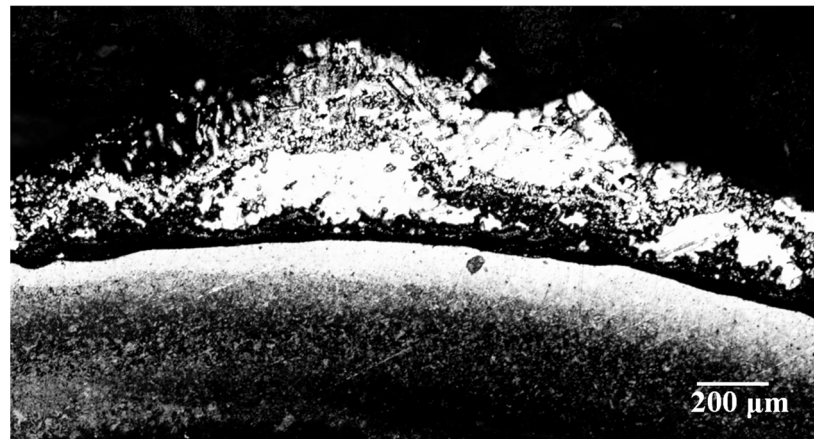


Figure 18. Microstructure characteristics of the area near the welding spot.

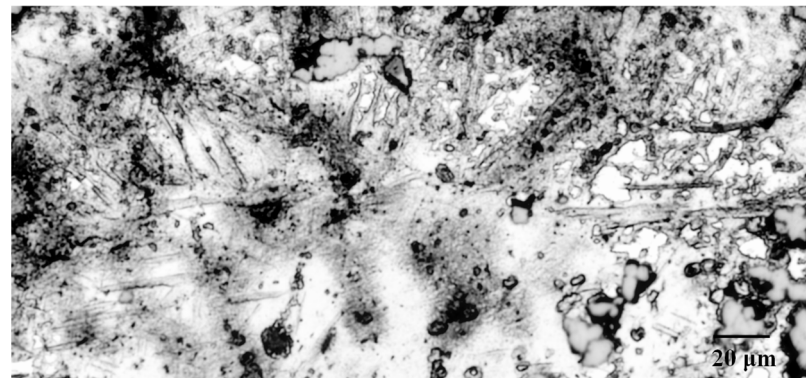


Figure 19. Metallographic structure characteristics of welding spot.



Figure 20. Metallographic structure characteristics in normal area.

4. Conclusions

- (1) Defects of scratches, abrasions and welding spots inevitably occur during processing and installation of the HVFLC. Defects can damage the Zn-5%Al-rare earth alloy coating on the surface of the wires. It will negatively affect the mechanical properties and corrosion resistance of the HVFLC, and adversely affect the long-term service performance.
- (2) The accelerated corrosion tests with corrosion paste showed that the presence of scratch, abrasion and welding spot damaged the Zn-5% Al-rare earth alloy coating

on the surface of the HVFLC. Different effects on the corrosion resistance of the wires were observed. The effect of welding spot defects is the most serious, and the corrosion mechanism and pattern still need further study.

- (3) It can be found from the mechanical tensile test that the mechanical properties of the HVFLC were affected by various defects. Stress concentration occurs during tension due to surface defects of specimens. Defected specimens are more likely to fail under tension than standard specimens with a complete alloy coating. In addition, the presence of welding spot defects changed the metallographic structural characteristics of the specimens. A hard brittle martensite structure with poor toughness was produced in these areas. The mixed fractures of brittle fractures and ductile fractures occur in the specimens. Additionally, the tensile strength of the specimens decreases by about 40%.
- (4) Defects causing damage to alloy coating should be avoided as far as possible during processing and application of the HVFLC. Defects of welding spots have a great influence on corrosion resistance and mechanical properties. In order to guarantee the long-term service performance of the cable body, it is necessary to prevent the occurrence of welding spots.

Author Contributions: Writing—original draft preparation, Z.F.; conceptualization, J.F., Z.W. and B.C.; writing—review and editing, Z.F. and J.F.; experiment, P.S. and J.M. All authors have read and agreed to the published version of the manuscript.

Funding: This research was funded by No. 13th Five-Year national key research and development program-Technology Winter Games-the research and demonstration of the key technology for the construction and application of the NSSO (2019YFF0301500)/ the Special Financial Science and Technology Project in Xicheng District of Beijing-Research on Key Technology of Domestic High-Vanadium Full-Locked Cable in the NSSO of Winter Olympic Games (XCSTS-TI2021-29)/ the talent introduction project of Beijing University of Chemical Technology (BUCTRC202026).

Data Availability Statement: The data presented in this study are available in the chart in this paper.

Acknowledgments: The support of No. 13th Five-Year national key research and development program-Technology Winter Games-the research and demonstration of the key technology for the construction and application of the NSSO (2019YFF0301500), the Special Financial Science and Technology Project in Xicheng District of Beijing-Research on Key Technology of Domestic High-Vanadium Full-Locked Cable in the NSSO of Winter Olympic Games (XCSTS-TI2021-29), the talent introduction project of Beijing University of Chemical Technology (BUCTRC202026) are much appreciated.

Conflicts of Interest: The authors declare no conflict of interest.

References

1. Yang, Y.C.; Chen, B.L. Design of main structure of national speed skating Hall. *Build. Struct.* **2018**, *48*, 1–4.
2. Wang, Z.; Bai, G.B. Steel structural design of National Speed Skating Oval. *Build. Struct.* **2018**, *48*, 5–11.
3. Zhang, J.X.; Gao, S.D.; Wang, Z.Q. Key Construction Technology of Long-span Saddleback Cable Network Structure of National Speed Skating Oval. *Constr. Technol.* **2019**, *48*, 41–44.
4. Bai, G.B.; Wang, Z. Key Issues in Cable Net Form-Finding of the National Speed Skating Oval. *Steel Constr.* **2020**, *35*, 54–61.
5. Zhang, Y.; Su, Z.H. Manufacture Technologies of High-Vanadium Full-Locked Cable Used in National Speed Skating Oval Project. *Constr. Technol.* **2020**, *49*, 7–11.
6. GB/T 6465-2008; Metallic and Other Non-Organic Coatings-Corrodokote Corrosion Test (CORR Test). Standard GB: Beijing, China, 2008.
7. Wang, X.F.; Liu, H. Effect of welding method on defect, microstructure and mechanical properties of welded joints of Q235 steel. *Trans. Mater. Heat Treat.* **2021**, *42*, 150–159.
8. Chen, L.; Nie, P.; Qu, Z.; Ojo, O.A.; Xia, L.; Li, Z.; Huang, J. Influence of heat input on the changes in the microstructure and fracture behavior of laser welded 800MPa grade high-strength low-alloy steel. *J. Manuf. Processes* **2020**, *50*, 132–141. [[CrossRef](#)]
9. Song, S.K.; Feng, Y. Correlativity on corrodokote accelerated corrosion test and atmospheric exposure test of pure aluminum 1060. *Light Met.* **2018**, *2*, 54–58.
10. Han, G.M. *Theory and Technology of Welding Process*; China Machine Press: Beijing, China, 2018.

11. Li, Y.J.; Wang, J. *Welding Defect Analysis and Countermeasures*; Chemical Industry Press: Beijing, China, 2018.
12. Bai, L.Y.; Jiang, K.B.; Gao, L. The Influence and Mechanism of Residual Stress on the Corrosion Behavior of Welded Structures. *Mater. Res.* **2018**, *21*, e20180166. [[CrossRef](#)]